This article has been accepted for publication in IEEE Transactions on Signal Processing. This is the author's version which has not been fully edited and content may change prior to final publication. Citation information: DOI 10.1109/TSP.2024.3366438

FDA-MIMO Transmitter and Receiver Optimization

Lan Lan, *Member, IEEE*, Massimo Rosamilia, *Member, IEEE*, Augusto Aubry, *Senior Member, IEEE*, Antonio De Maio, *Fellow, IEEE*, and Guisheng Liao, *Senior Member, IEEE*

***Abstract*—This paper addresses the joint design of the transmit parameters (i.e., radar code/frequency increments) and the receive filter in a Frequency Diverse Array (FDA)-Multiple-Input Multiple-Output (MIMO) radar system. The operating environment includes clutter, namely signal-dependent interference tied up to the FDA transmitted waveforms and the antenna array features, along with conventional thermal noise. The chosen optimization policy relies on the constrained maximization of the Signal-to-Interference-plus-Noise Ratio (SINR) which for Gaussian interference is tantamount to maximizing the radar detection performance. In this context, a bespoke Minorization-Maximization (MM)-Maximum Block Improvement (MBI) algorithm is proposed to tackle the resulting constrained non-convex optimization problem. The convergence properties of the resulting procedure are rigorously proven, along with a thorough investigation of the computational complexity for its implementation. Finally, numerical results are provided to show the effectiveness of the new technique under diverse clutter scenarios of practical relevance and in comparison with some counterparts.**

***Index Terms*—FDA-MIMO radar, joint transmit and receive optimization, signal-dependent interference, clutter, MBI.**

I. Introduction

Amid the ever-evolving landscape of radar technology, the development of advanced techniques capable of ensuring adequate performance, even in adverse operating conditions, is noteworthiness. In this context, the presence of signal-dependent interference (environmental reverberation, i.e., clutter) stands out as a primary issue worthy of research efforts [1]–[5]. In particular, to cope with this challenging self-induced disturbance, the design of bespoke transceivers is a pivotal strategy, employed by plenty of literature works aimed at maximizing the Signal-to-Interference-plus-Noise Ratio (SINR) at the receiving end, encompassing some *a priori* knowledge about the operating environment [3], [6]–[10]. Precisely, appropriate waveform design problems, with the goal of optimizing the radar code and the receive filter, are proposed to enhance the detection performance while guaranteeing the fulfillment of specific key requirements, in terms of constraints about waveforms modulus and similarities to some reference signals [11]–[13], Peak-to-Average-power Ratio [14], and finite energy [2].

Notably, the waveform design task typically involves solving an NP-hard optimization problem due to the numerous constraints. To devise practically implementable procedures capable of yielding good quality solutions with a limited resource demand, several solution strategies based on the Majorization-Minimization (MM) method [15], sequential optimization [16], relaxation and matrix decomposition [17], and Coordinate Descent (CD) [18], have been proposed in the open literature [2], [7], [19]–[22]. Remarkably, such optimization techniques have also been successfully applied to waveform design problems using Multiple-Input Multiple-Output (MIMO) radars operating in the presence of signal-dependent interference, exploiting the underlying waveform diversity [23]–[30].

Aside from the conventional radar (such as the phased array and MIMO), the Frequency Diverse Array (FDA) radar has recently emerged as a novel and promising technology. In a nutshell, by leveraging proper carrier shifts at each transmit array element, such radar encompasses a range-angle-time-dependent transmit beampattern [31]. Capitalizing on this characteristic, suitable resource allocation strategies have been proposed in the open literature. Specifically, the joint design of transmit and receive weights for coherent FDA radar is investigated in [32], considering both energy and similarity constraints, to maximize the power toward a specific area in the range-angle domain. The problem is then solved via a sequential optimization method based on SemiDefinite Relaxation. Furthermore, in [33], by optimizing both the weight vector and the frequency increments, an adaptive approach for target localization with an FDA radar is developed according to a bespoke Bayesian criterion.

To overcome some challenges of the legacy FDA technology, its combination with the MIMO paradigm has been conceived giving rise to the so-called FDA-MIMO radar [34], [35], widely investigated in the open literature for solving important issues such as suppression of mainlobe deceptive jammers [36] and clutter [37], just to mention a few. Differently from traditional Space-Time Adaptive Processing (STAP)-based methods, the FDA-MIMO can distinguish echoes from different range ambiguity regions, allowing it to cope with the problem of range-dependent and range-ambiguous clutter suppression [37]–[39]. Indeed the dependency of the steering vector on the incremental range, i.e., the target displacement with respect to (w.r.t.) the center of the occupied range cell, is a peculiarity of the FDA-MIMO architecture [34]. It paves the way to new processing frontiers and it does not arise in a conventional colocated MIMO radar. Along this line, in [37], an enhanced Three-Dimensional (3D) localization technique,

This work of Lan Lan was supported in part by the National Nature Science Foundation of China (Nos. 62101402, 61931016), China Postdoctoral Science Foundation (Nos. 2021TQ0261, 2021M702547), the Science and Technology Innovation Team of Shaanxi Province (No. 2022TD-38), and the Basic Science Research Fund in Xidian University (No. QTZX23068).

Lan Lan and Guisheng Liao are with the National Key Laboratory of Radar Signal Processing, Xidian University, Xi'an 710071, China. E-mail: lanlan@xidian.edu.cn, liaogs@xidian.edu.cn

Massimo Rosamilia, Augusto Aubry, and Antonio De Maio are with Università degli Studi di Napoli "Federico II", DIETI, Via Claudio 21, I-80125 Napoli, Italy and with the National Inter-University Consortium for Telecommunications, 43124 Parma, Italy. E-mail: massimo.rosamilia@unina.it, augusto.aubry@unina.it, ademaio@unina.it (Corresponding author: Antonio De Maio.)

This article has been accepted for publication in IEEE Transactions on Signal Processing. This is the author's version which has not been fully edited and content may change prior to final publication. Citation information: DOI 10.1109/TSP.2024.3366438

with limited processing complexity, is proposed in an airborne FDA-MIMO radar. In addition, a two-stage adaptive clutter suppression method is developed in [38], encompassing a multi-waveform based adaptive beamforming followed by a tailored STAP processing that capitalizes on auxiliary beams. In [39], an FDA-MIMO-based bistatic radar configuration is considered, thereby addressing the clutter discrimination and suppression tasks using a 3D localized space-time-range adaptive processing method.

Notably, the joint optimization of transmit and receive parameters for an FDA-MIMO architecture has only received limited attention. In [40], an iterative algorithm is derived to improve the SINR by optimizing the transmit beamspace and receive filter, considering constant energy constraints. A cognitive transmit and receive filter design, considering a moving target detection scenario, is proposed in [41].

That said, the joint optimization of the frequency increments, radar code, and receiver filter, in an FDA-MIMO radar system has not already been addressed, especially for improving the detection performance in the presence of signal-dependent clutter. In this regard, capitalizing on *a priori* knowledge of the environment surrounding the radar, the problem of maximizing the SINR at the output of the receive filter is studied. Precisely, a joint optimization strategy of the transmit parameters (i.e., radar code/frequency increments) and the receive architecture is conceived, including, at the design stage, specific constraints stemming from practical and physical limitations as well as desired operational behavior. Therefore, energy and similarity constraints [13] are imposed in the code optimization, to control some specific characteristics of the transmitted waveforms [7], [21]. Furthermore, boundaries to frequency increments are considered as a result of the limited available radar bandwidth.

Due to the nature of the objective function and the aforementioned constraints, the successful accomplishment of the pursued task is tied up to the solution of a non-convex NP-hard optimization problem. Thus, a tailored MM-Maximum Block Improvement (MBI) [42] procedure is developed and analyzed.

To summarize, the main technical contributions of this paper are:

- The SINR maximization problem is formulated as a constrained optimization problem, in which the frequency increments, the code, and the filter are jointly optimized by leveraging *a priori* information about the clutter statistics while fulfilling specific constraints.
- To tackle the NP-hard optimization problem, an MM-MBI solution strategy is devised. It involves the solution of subproblems, one for each variables block, i.e., the i-th frequency offset, code, and filter, which are either optimally solved (using for instance state of the art matrix decomposition tools [43]) or handled resorting to the MM paradigm. In this last situation, an important result is represented by the construction of bespoke surrogate functions ensuring some peculiar analytic properties necessary to make convergence claims.
  At a given iteration, the MBI updates the variable block related to the highest increment (in terms of achieved SINR), while keeping the other blocks fixed to their previous values.
- The convergence properties of the proposed algorithm are thoroughly analyzed, proving that any cluster point of the optimization sequence satisfies the Karush-Kuhn-Tucker (KKT) condition [44].
- The computational complexity of the proposed procedure is thoroughly discussed, providing a detailed analysis for the solution of each subproblem.
- Numerical results are presented aimed at corroborating the theoretical achievements under diverse clutter scenarios of practical relevance, also in comparison with an Alternating Optimization (AO)-based procedure and some simpler MBI-based optimization approaches, which do not exploit all the available degrees of freedom (DOF)s.

The paper is organized as follows. In Section II, the signal model of FDA-MIMO radar operating in a background of signal-dependent clutter is introduced. In Section III, a transceiver design approach based on the joint optimization of transmit parameters (radar code and frequency increments) and receive filter is formulated. Moreover, an MM-MBI algorithm is developed to tackle the constrained optimization problem. The convergence properties and the corresponding computational complexity are then thoroughly discussed. Numerical results are presented in Section IV, whereas conclusions and possible future research avenues are provided in Section V.

A. Notations

Boldface is used for vectors $\boldsymbol{a}$ (lower case), and matrices $\boldsymbol{A}$ (upper case). The (k,l)-entry (or l-entry) of a generic matrix $\boldsymbol{A}$ (or vector $\boldsymbol{a}$) is indicated as $\boldsymbol{A}(k,l)$ (or a_l). $\boldsymbol{I}$ and $\mathbf{0}$ denote respectively the identity matrix and the matrix with zero entries (their size is determined from the context). The all-ones column vector of size N is denoted by $\mathbf{1}_N$, whereas $\boldsymbol{e}_k$ denotes the k-th column vector of $\boldsymbol{I}$, whose size is determined from the context. Additionally, $\mathrm{diag}(\boldsymbol{x})$ indicates the diagonal matrix whose i-th diagonal element is $\boldsymbol{x}(i)$. The transpose and the conjugate transpose operators are denoted by the symbols $(\cdot)^{\mathrm{T}}$ and $(\cdot)^{\dagger}$, respectively. $\odot$, and $\otimes$ represent the Hadamard (element-wise) product, and Kronecker product, respectively. The trace and the rank of the matrix $\boldsymbol{A} \in \mathbb{C}^{N\times N}$ are indicated with $\mathrm{tr}\{\boldsymbol{A}\}$ and $\mathrm{Rank}(\boldsymbol{A})$, respectively. $\mathbb{R}^N$ and $\mathbb{C}^N$ are respectively the sets of N-dimensional column vectors of real and complex numbers. $\mathbb{H}^N$ represents the set of $N \times N$ Hermitian matrices. The letter j refers to the imaginary unit (i.e., $j = \sqrt{-1}$). For any complex number x, $|x|$ indicates the modulus of x and $\mathrm{Re}\{x\}$ denotes its real part. Moreover, for any $\boldsymbol{x} \in \mathbb{C}^N$, $\|\boldsymbol{x}\|$ denotes the Euclidean norm. $\mathbb{E}[\cdot]$ denotes the statistical expectation. Furthermore, for any $x, y \in \mathbb{R}$, $\max(x,y)$ returns the maximum between the two arguments. Finally, for any optimization problem $\mathcal{P}$, $\upsilon(\mathcal{P})$ represents its optimal value.

II. System Model of FDA-MIMO Radar

Let us consider an FDA-MIMO system with M transmit and N receive antenna elements, where frequency increments are introduced across the transmit array elements, i.e.,

This article has been accepted for publication in IEEE Transactions on Signal Processing. This is the author's version which has not been fully edited and content may change prior to final publication. Citation information: DOI 10.1109/TSP.2024.3366438

$\boldsymbol{\Delta f} = [\Delta f_1, \Delta f_2, \ldots, \Delta f_M]^{\mathrm{T}} \in \mathbb{R}^M$. Specifically, the carrier frequency of the m-th ($m = 1, \ldots, M$) transmit element is assigned as

$$f_m = f_0 + \Delta f_m, \tag{1}$$

where f_0 indicates the reference carrier[1].

Let $\boldsymbol{c} = [c_1, c_2, \ldots, c_P]^{\mathrm{T}} \in \mathbb{C}^P$ be the transmitted radar code vector modulating the fast time probing signals[2] with $P \geq 3$ the number of coded sub-pulses (code length). Then, the waveform at the receiver end is down-converted to baseband, undergoes a tuned pulse matched filtering operation, and then is sampled. The fast-time observations from the range-azimuth Cell Under Test (CUT) are collected in the vector $\boldsymbol{v} \in \mathbb{C}^{PMN}$, which can be expressed as [7]

$$\boldsymbol{v} = \boldsymbol{z}_{\mathrm{S}} + \boldsymbol{z}_{\mathrm{C}} + \boldsymbol{n}, \tag{2}$$

where

- $\boldsymbol{z}_{\mathrm{S}} \in \mathbb{C}^{PMN}$ denotes the vector of the samples from a prospective target within the CUT, namely,

$$\boldsymbol{z}_{\mathrm{S}} = \alpha_0 \boldsymbol{c} \otimes \boldsymbol{s}(\theta_0, \Delta\tau, \boldsymbol{\Delta f}), \tag{3}$$

  with
  - α_0 the complex coefficient accounting for target backscattering and the other terms involved in the two-way radar equation;
  - θ_0 the azimuth of the target;
  - $\Delta\tau$ the incremental range of the target within the range cell, which accounts for the difference between the sampling instant $t^\star$ and the actual target range $\tau_0 = 2R_0/c$, i.e., $\Delta\tau = t^\star - \tau_0 = t_1^\star$, with R_0 the target range [34];
  - $\boldsymbol{s}(\theta_0, \Delta\tau, \boldsymbol{\Delta f}) \in \mathbb{C}^{MN}$ the joint transmit-receive steering vector, which can be further written as [45]

$$\boldsymbol{s}(\theta_0, \Delta\tau, \boldsymbol{\Delta f}) = \boldsymbol{d}(\theta_0) \otimes [\boldsymbol{a}(\theta_0) \odot \boldsymbol{b}(\Delta\tau, \boldsymbol{\Delta f})], \tag{4}$$

    with
    - $\boldsymbol{d}(\theta_0) = \left[1, e^{j2\pi \frac{d}{\lambda_0} \sin(\theta_0)}, \cdots, e^{j2\pi \frac{d}{\lambda_0}(N-1)\sin(\theta_0)}\right]^{\mathrm{T}} \in \mathbb{C}^N$ the angle-dependent receive steering vector, d the array interelement spacing, and λ_0 the reference carrier wavelength;
    - $\boldsymbol{a}(\theta_0) = \boldsymbol{R}^{\mathrm{T}} \left[1, e^{j2\pi \frac{d}{\lambda_0} \sin(\theta_0)}, \cdots, e^{j2\pi \frac{d}{\lambda_0}(M-1)\sin(\theta_0)}\right]^{\mathrm{T}} \in \mathbb{C}^M$ the angle-dependent transmit steering vector;
    - $\boldsymbol{b}(\Delta\tau, \boldsymbol{\Delta f}) = \left[e^{j2\pi\Delta\tau\Delta f_1}, \ldots, e^{j2\pi\Delta\tau\Delta f_M}\right]^{\mathrm{T}} \in \mathbb{C}^M$ the range-dependent transmit steering vector, with $\boldsymbol{R}$ the covariance matrix of the basic set of transmitted pulses;
- $\boldsymbol{z}_{\mathrm{C}} \in \mathbb{C}^{PMN}$ contains the filtered clutter samples from the range-azimuth bins adjacent to the CUT (as depicted in Fig. 1), which is the superposition of the returns from different uncorrelated scatterers, i.e.,

$$\boldsymbol{z}_{\mathrm{C}} = \sum_{l=-L+1}^{L-1} \sum_{i=0}^{I-1} \sum_{k=1}^{K} \beta_{l,i,k} \boldsymbol{J}_l \boldsymbol{c} \otimes \boldsymbol{s}(\theta_i, \Delta\tau_k, \boldsymbol{\Delta f}), \tag{5}$$

  with
  - $2L-2$ ($L \leq P$) the number of range rings that interfere with the range-azimuth bin of interest, i.e., $(l, i) = (0, 0)$;
  - I the number of discrete azimuth sectors [42];
  - K the maximum number of the scatterers within a single range-azimuth bin;
  - $\Delta\tau_k$ and θ_i refer to the incremental range and azimuth, respectively, of the k-th ($k = 1, \ldots, K$) scatterer from the i-th ($i = 1, \ldots, I$) azimuth sector and a generic range ring (without loss of generality, the same range displacements are considered among the different range bins);
  - $\boldsymbol{J}_l \in \mathbb{R}^{P \times P}$ the binary shift matrix with ones only on its l-th ($l = 0, \pm1, \pm2, \ldots, \pm(P-1)$) diagonal ($l$ indicates the range ring), and zeros elsewhere, i.e.,

$$\boldsymbol{J}_l(p, q) = \begin{cases} 1, p - q = l \\ 0, \text{elsewhere} \end{cases}, \quad (p, q) \in \{1, \ldots, P\}^2, \tag{6}$$

    with $\boldsymbol{J}_0 = \boldsymbol{I}$;
  - $\beta_{l,i,k}$ the backscattering amplitude of the k-th scatterer from the (l, i)-th range-azimuth bin (with $\beta_{l,i,k} = 0 \ \forall k$ when $l = 0$ and $i = 0$), which are modeled as independent complex, zero-mean, circularly symmetric, random variables with $\mathbb{E}[|\beta_{l,i,k}|^2] = \sigma_{l,i,k}^2$, whose actual value can be inferred exploiting some a-priori information on the illuminated scene [7], [46]. As a result, the covariance matrix of $\boldsymbol{z}_{\mathrm{C}}$ can be evaluated as

$$\begin{aligned} \boldsymbol{\Sigma}_{\mathrm{c}}(\boldsymbol{c}, \boldsymbol{\Delta f}) &= \mathbb{E}[\boldsymbol{z}_{\mathrm{C}} \boldsymbol{z}_{\mathrm{C}}^\dagger] \\ &= \sum_{l=-P+1}^{P-1} \sum_{i=0}^{I-1} \sum_{k=1}^{K} \sigma_{l,i,k}^2 \bar{\boldsymbol{\Gamma}}_l(\boldsymbol{c}, \theta_i, \Delta\tau_k, \boldsymbol{\Delta f}) \\ &\in \mathbb{C}^{PMN \times PMN}, \end{aligned} \tag{7}$$

    with $\bar{\boldsymbol{\Gamma}}_l(\boldsymbol{c}, \theta_i, \Delta\tau_k, \boldsymbol{\Delta f}) \in \mathbb{C}^{PMN \times PMN}$ given by

$$\begin{aligned} &\bar{\boldsymbol{\Gamma}}_l(\boldsymbol{c}, \theta_i, \Delta\tau_k, \boldsymbol{\Delta f}) = \\ &\left(\boldsymbol{J}_l \boldsymbol{c} \boldsymbol{c}^\dagger \boldsymbol{J}_l^\dagger\right) \otimes \left(\boldsymbol{s}(\theta_i, \Delta\tau_k, \boldsymbol{\Delta f}) \boldsymbol{s}^\dagger(\theta_i, \Delta\tau_k, \boldsymbol{\Delta f})\right); \end{aligned} \tag{8}$$

- $\boldsymbol{n} \in \mathbb{C}^{PMN}$ comprises the internal noise, which is modeled as a zero-mean, complex, circularly symmetric, Gaussian random vector, i.e., $\mathbb{E}[\boldsymbol{n}] = 0$ and covariance $\mathbb{E}[\boldsymbol{n}\boldsymbol{n}^\dagger] = \sigma_n^2 \boldsymbol{I}$ with σ_n^2 the noise power level (assumed without loss of generality equal to 0 dB).

III. Joint Transmit and Receive Filter Design Problem

An FDA-MIMO radar tranceiver design approach is introduced via the joint optimization of the transmit DOFs (radar code/frequency increments) and receive filter, aimed at maximizing the SINR while controlling some hallmarks of the

[1]Notice that in a plain FDA-MIMO, the carrier frequencies of transmit elements are linearly increased, namely, $f_m = f_0 + (m-1)\Delta f$, with an identical relative increment Δf.

[2]The transmit signal on a given antenna is obtained concatenating P waveforms described in [34] for each specific element after amplitude/phase modulation with a common sequence.

This article has been accepted for publication in IEEE Transactions on Signal Processing. This is the author's version which has not been fully edited and content may change prior to final publication. Citation information: DOI 10.1109/TSP.2024.3366438

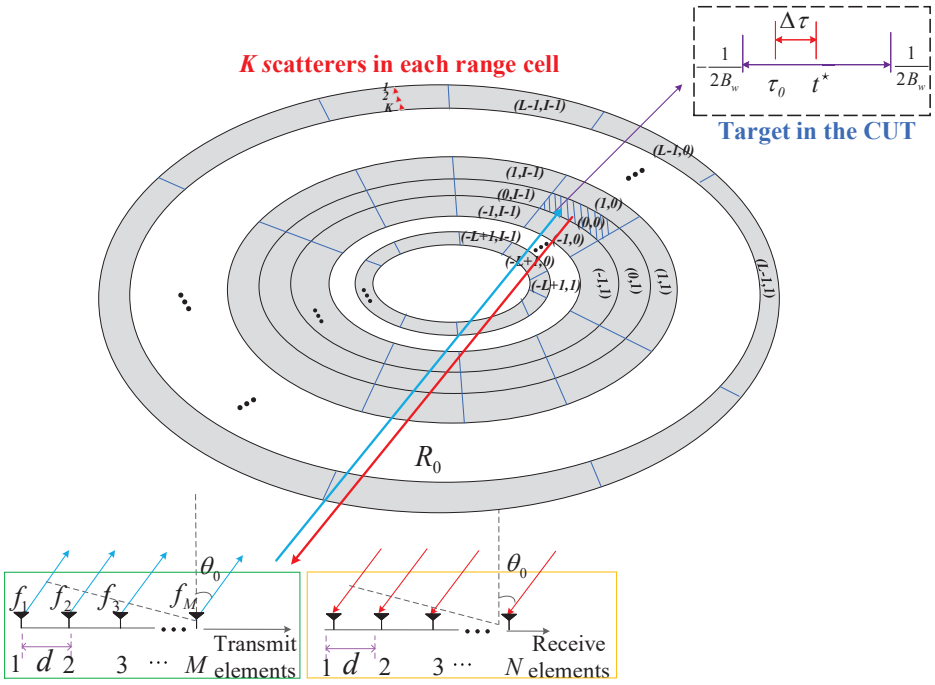

Fig. 1: Geometry of the FDA and range-azimuth bins contributing to the return from the CUT. The generic (l, i) indexes the l-th range and i-th azimuth pair.

transmitted waveform via tailored constraints on the probing code and frequency increments, as thoroughly discussed below.

1) Energy Constraint: To comply with the radar power budget, the energy constraint is forced on the sought code to account for the finite energy transmitted by the radar, which is tantamount to forcing

$$\|\boldsymbol{c}\|^2 = 1. \tag{9}$$

2) Similarity Constraint: To bestow some desirable attributes to the radar probing code, a similarity constraint is imposed on the transmitted sequence, i.e.,

$$\|\boldsymbol{c} - \boldsymbol{c}_0\|^2 \leq \delta, \tag{10}$$

where $0 < \delta < 2$ rules the size of the similarity region, and $\boldsymbol{c}_0 \in \mathbb{C}^P$ represents a reference code ($\|\boldsymbol{c}_0\| = 1$), which possesses some desired features from the radar performance point of view (as for instance limited amplitude variation of the elements).

3) Spectral bandwidth occupancy constraint: Without loss of generality, each frequency increment is supposed to satisfy

$$0 \leq \Delta f_m \leq B_w, \ m = 1, \ldots, M, \tag{11}$$

where B_w denotes the available radar bandwidth for the selection of the transmit frequencies and $B_w + B_c$ the overall single-side radar bandwidth with B_c the sub-pulse bandwidth.

Now, supposing the received signal $\boldsymbol{v}$ filtered via $\boldsymbol{w} \in \mathbb{C}^{PMN}$, the chosen figure of merit is the normalized (w.r.t. $|\alpha_0|^2$) SINR at the output of the receive filter, which is given by

$$\mathrm{SINR}(\boldsymbol{w}, \boldsymbol{c}, \boldsymbol{\Delta f}) = \frac{|\boldsymbol{w}^\dagger (\boldsymbol{c} \otimes \boldsymbol{s}(\theta_0, \Delta\tau, \boldsymbol{\Delta f}))|^2}{\boldsymbol{w}^\dagger \boldsymbol{\Sigma}_c(\boldsymbol{c}, \boldsymbol{\Delta f}) \boldsymbol{w} + \sigma_n^2 \|\boldsymbol{w}\|^2}. \tag{12}$$

Hence, the joint transmit receive design problem can be cast as the following constrained optimization problem

$$\mathcal{P}: \begin{cases} \max\limits_{\boldsymbol{c}, \boldsymbol{w}, \Delta f_1, \ldots, \Delta f_M} & \mathrm{SINR}(\boldsymbol{w}, \boldsymbol{c}, \boldsymbol{\Delta f}) \\ \text{s.t.} & 0 \leq \Delta f_m \leq B_w, \ m = 1, \cdots, M \\ & \|\boldsymbol{c}\|^2 = 1 \\ & \|\boldsymbol{c} - \boldsymbol{c}_0\|^2 \leq \delta \\ & \|\boldsymbol{w}\|^2 = 1 \end{cases}. \tag{13}$$

Notice that $\mathcal{P}$ is a non-convex and in general NP-hard optimization problem. To come up with good quality suboptimal solutions, a sequential optimization procedure is designed resorting to a MM-MBI paradigm [42], [47]–[49]. In a nutshell, it partitions the vector variable into multiple blocks, and then the assessment of the objective function improvement (either optimized or handled with MM) w.r.t. each block, while keeping the others fixed, is performed. In particular, at each iteration only the block yielding the maximum increase of the objective function is updated. To proceed further with the algorithm development, let us introduce the vector $\boldsymbol{y}$ collecting all the optimization variables, i.e.,

$$\boldsymbol{y} = \left[\boldsymbol{w}^{\mathrm{T}}, \boldsymbol{c}^{\mathrm{T}}, (\Delta f_1, \ldots, \Delta f_M)^{\mathrm{T}}\right]^{\mathrm{T}} \in \mathbb{C}^{PMN+P+M}, \tag{14}$$

which is partitioned into $M + 2$ blocks given by $\boldsymbol{y}_1, \boldsymbol{y}_2, y_3, \ldots, y_{M+2}$, with $\boldsymbol{y}_1 = \boldsymbol{w} \in \mathbb{C}^{PMN}$, $\boldsymbol{y}_2 = \boldsymbol{c} \in \mathbb{C}^P$, and $y_h = \Delta f_{h-2}, (h = 3, \ldots, M + 2)$ corresponding to the receive filter, radar code, and frequency increments to be optimized, respectively. Moreover, the optimization vector obtained at the $(n-1)$-th iteration is denoted by

$$\boldsymbol{y}^{(n-1)} = \left[\boldsymbol{w}^{(n-1)\mathrm{T}}, \boldsymbol{c}^{(n-1)\mathrm{T}}, (\Delta f_1^{(n-1)}, \ldots, \Delta f_M^{(n-1)})^{\mathrm{T}}\right]^{\mathrm{T}}. \tag{15}$$

The application of the procedure requires handling $M + 2$

sub-problems at each iteration [18], namely,

$$\mathcal{P}_{\Delta f_m^{(n)}}\colon \begin{cases} \max\limits_{\Delta f_m} & \mathrm{SINR}\left(\boldsymbol{w}^{(n-1)}, \boldsymbol{c}^{(n-1)}, \widetilde{\boldsymbol{\Delta f}}_m\right) \\ \text{s.t.} & 0 \le \Delta f_m \le B_w \end{cases}, \quad (16)$$

for $m = 3, \ldots, M+2$,

$$\mathcal{P}_{\boldsymbol{c}^{(n)}}\colon \begin{cases} \max\limits_{\boldsymbol{c}} & \mathrm{SINR}\left(\boldsymbol{w}^{(n-1)}, \boldsymbol{c}, \boldsymbol{\Delta f}^{(n-1)}\right) \\ \text{s.t.} & \|\boldsymbol{c}\|^2 = 1 \\ & \|\boldsymbol{c} - \boldsymbol{c}_0\|^2 \le \delta \end{cases}, \quad (17)$$

and

$$\mathcal{P}_{\boldsymbol{w}^{(n)}}\colon \begin{cases} \max\limits_{\boldsymbol{w}} & \mathrm{SINR}\left(\boldsymbol{w}, \boldsymbol{c}^{(n-1)}, \boldsymbol{\Delta f}^{(n-1)},\right) \\ \text{s.t.} & \|\boldsymbol{w}\|^2 = 1 \end{cases}, \quad (18)$$

where

- $\widetilde{\boldsymbol{\Delta f}}_m = \left[\Delta f_1^{(n-1)}, \ldots, \Delta f_{m-1}^{(n-1)}, \Delta f_m, \Delta f_{m+1}^{(n-1)}, \cdots, \Delta f_M^{(n-1)}\right]^{\mathrm{T}} \in \mathbb{R}^M$ (the m-th element is the optimization variable);
- $\boldsymbol{\Delta f}^{(n-1)} = \left[\Delta f_1^{(n-1)}, \ldots, \Delta f_M^{(n-1)}\right]^{\mathrm{T}} \in \mathbb{R}^M$.

From an analytical point of view, $\Delta f_m^{(n)}$, $\boldsymbol{c}^{(n)}$, and $\boldsymbol{w}^{(n)}$ are suitable feasible points (either optimal or bespoke sub-optimal) to the sub-problems $\mathcal{P}_{\Delta f_m^{(n)}}$ $(m = 1, \ldots, M)$, $\mathcal{P}_{\boldsymbol{c}^{(n)}}$, and $\mathcal{P}_{\boldsymbol{w}^{(n)}}$, respectively.

In the devised optimization procedure, the problems $\mathcal{P}_{\Delta f_m^{(n)}}$ $(m = 1, \ldots, M)$ are dealt with in Subsection III-A, resorting to the MM approach with the final goal to improve the objective. Problems $\mathcal{P}_{\boldsymbol{c}^{(n)}}$ and $\mathcal{P}_{\boldsymbol{w}^{(n)}}$ are hidden convex. Specifically, an optimal solution to $\mathcal{P}_{\boldsymbol{c}^{(n)}}$ can be found via a polynomial-time method [7], while an optimal solution to the problem $\mathcal{P}_{\boldsymbol{w}^{(n)}}$ is presented in closed form in Section III-C.

A. Frequency Increment Optimization

In this subsection, the m-th frequency increment Δf_m is optimized given the receive filter, radar code, and the other $M-1$ frequency increments. To proceed further, the following Lemma is provided, to come up with an alternative expression of the objective SINR in (12).

Lemma 1: An equivalent expression of the objective function in (16) is

$$\mathrm{SINR}\left(\boldsymbol{w}^{(n-1)}, \boldsymbol{c}^{(n-1)}, \widetilde{\boldsymbol{\Delta f}}_m\right) = \frac{\boldsymbol{b}_0^{\dagger}(\widetilde{\boldsymbol{\Delta f}}_m)\boldsymbol{W}\left(\boldsymbol{w}^{(n-1)}, \boldsymbol{c}^{(n-1)}\right)\boldsymbol{b}_0(\widetilde{\boldsymbol{\Delta f}}_m)}{\sum\limits_{k=1}^{K}\boldsymbol{b}_k^{\dagger}(\widetilde{\boldsymbol{\Delta f}}_m)\boldsymbol{\Sigma}_k\left(\boldsymbol{w}^{(n-1)}, \boldsymbol{c}^{(n-1)}\right)\boldsymbol{b}_k(\widetilde{\boldsymbol{\Delta f}}_m) + \sigma_n^2\|\boldsymbol{w}^{(n-1)}\|^2}, \quad (19)$$

where $\boldsymbol{b}_0(\widetilde{\boldsymbol{\Delta f}}_m) = \boldsymbol{b}(\Delta\tau, \widetilde{\boldsymbol{\Delta f}}_m)$ and $\boldsymbol{b}_k(\widetilde{\boldsymbol{\Delta f}}_m) = \boldsymbol{b}(\Delta\tau_k, \widetilde{\boldsymbol{\Delta f}}_m)$ while $\boldsymbol{W}\left(\boldsymbol{w}^{(n-1)}, \boldsymbol{c}^{(n-1)}\right) \in \mathbb{C}^{M\times M}$ and $\boldsymbol{\Sigma}_k\left(\boldsymbol{w}^{(n-1)}, \boldsymbol{c}^{(n-1)}\right) \in \mathbb{C}^{M\times M}$ are provided in eq. (46) and eq. (48) of Appendix A in the supplemental material, respectively.

Proof: See Appendix A of the supplemental material. ■

In order to tackle the sub-problem at hand, a MM approach is developed, whereby an appropriate tight minorant to the objective function at hand (constructed according to Proposition 1) is optimized to generate an updated solution.

Proposition 1: A tight minorant (surrogate) to the objective function in $\mathcal{P}_{\Delta f_m^{(n)}}$ is given by

$$\begin{aligned}&\widehat{\mathrm{SINR}}_a\left(\Delta f_m|\boldsymbol{\Delta f}^{(n-1)}, \boldsymbol{w}^{(n-1)}, \boldsymbol{c}^{(n-1)}\right) \\ &= X_m^{(n-1)}\Delta f_m^2 + \dot{\hat{X}}_m^{(n-1)}\Delta f_m + \dot{\bar{X}}_m^{(n-1)},\end{aligned} \quad (20)$$

with the specific definitions of $X_m^{(n-1)}$, $\dot{\hat{X}}_m^{(n-1)}$, and $\dot{\bar{X}}_m^{(n-1)}$ reported in Appendix B of the supplemental material.

Proof: The interested reader may refer to Appendix B of the supplementary material to this paper. ■

By leveraging Proposition 1, at the n-th iteration, the h-th $(h = 3, \ldots, M+2)$ sub-problem of the devised MM-MBI procedure becomes

$$\mathcal{P}_{y_h^{(n)}}\colon \begin{cases} \max\limits_{y_h} & \bar{\chi}_a\left(y_h; \boldsymbol{y}_h^{(n-1)}\right) \\ \text{s.t.} & y_h \in \Psi \end{cases}, \quad (21)$$

where $\bar{\chi}_a\left(y_h|\boldsymbol{y}_h^{(n-1)}\right)$ denotes $\widehat{\mathrm{SINR}}_a\left(\Delta f_m|\boldsymbol{\Delta f}^{(n-1)}, \boldsymbol{w}^{(n-1)}, \boldsymbol{c}^{(n-1)}\right)$ with reference to the variables introduced in (14) and (15), while the feasible set Ψ is given by

$$\Psi = \{x : 0 \le x \le B_w\}. \quad (22)$$

That said, a feasible solution to (21) is provided by the following proposition.

Proposition 2: The optimal solution to $\mathcal{P}_{y_h^{(n)}}$ is given by

$$\hat{y}_h = \max(\min(\tilde{y}_h, B_w), 0) \quad (23)$$

with

$$\tilde{y}_h = -\frac{\dot{\hat{X}}_m^{(n-1)}}{2X_m^{(n-1)}}. \quad (24)$$

Proof: See Appendix C of the supplemental material. ■

Hence, starting from $\boldsymbol{\Delta f}^{(n-1)}$, $\boldsymbol{w}^{(n-1)}$, and $\boldsymbol{c}^{(n-1)}$, the optimization of the h-th $(h = 3, \ldots, M+2)$ variable, i.e., y_h, can be accomplished according to (23).

B. Radar Code Optimization

In this subsection, the radar code is optimized with the frequency increments and receive filter fixed. First of all, using Lemma 2, an equivalent form of the objective function in (17) is obtained.

Lemma 2: An equivalent expression of the objective function in (17) is

$$\mathrm{SINR}\left(\boldsymbol{w}^{(n-1)}, \boldsymbol{c}, \boldsymbol{\Delta f}^{(n-1)}\right) = \frac{\boldsymbol{c}^{\dagger}\boldsymbol{\Theta}\left(\boldsymbol{w}^{(n-1)}, \boldsymbol{\Delta f}^{(n-1)}\right)\boldsymbol{c}}{\boldsymbol{c}^{\dagger}\boldsymbol{M}\left(\boldsymbol{w}^{(n-1)}, \boldsymbol{\Delta f}^{(n-1)}\right)\boldsymbol{c}}, \quad (25)$$

where the definitions of $\boldsymbol{\Theta}\left(\boldsymbol{w}^{(n-1)}, \boldsymbol{\Delta f}^{(n-1)}\right) \in \mathbb{C}^{P\times P}$ and $\boldsymbol{M}(\boldsymbol{w}^{(n-1)}, \boldsymbol{\Delta f}^{(n-1)}) \in \mathbb{C}^{P\times P}$ are given in Appendix D of the supplemental material.

Proof: See Appendix D of the supplemental material. ■

This article has been accepted for publication in IEEE Transactions on Signal Processing. This is the author's version which has not been fully edited and content may change prior to final publication. Citation information: DOI 10.1109/TSP.2024.3366438

In this regard, the problem $\mathcal{P}_{\boldsymbol{c}^{(n)}}$ is recast as

$$\mathcal{P}_{\boldsymbol{c}^{(n)}}\colon \begin{cases} \max\limits_{\boldsymbol{c}} & \mathrm{SINR}\left(\boldsymbol{w}^{(n-1)}, \boldsymbol{c}, \boldsymbol{\Delta f}^{(n-1)}\right) \\ \text{s.t.} & \|\boldsymbol{c}\|^2 = 1 \\ & \|\boldsymbol{c}-\boldsymbol{c}_0\|^2 \leq \delta \end{cases}, \tag{26}$$

which is a fractional quadratic optimization problem. Then, in terms of $\boldsymbol{y}_2$, it can be rewritten as

$$\mathcal{P}_{\boldsymbol{y}_2^{(n)}}\colon \begin{cases} \max\limits_{\boldsymbol{y}_2} & \frac{\boldsymbol{y}_2^\dagger \boldsymbol{\Theta}\left(\boldsymbol{w}^{(n-1)}, \boldsymbol{\Delta f}^{(n-1)}\right)\boldsymbol{y}_2}{\boldsymbol{y}_2^\dagger \boldsymbol{M}\left(\boldsymbol{w}^{(n-1)}, \boldsymbol{\Delta f}^{(n-1)}\right)\boldsymbol{y}_2} \\ \text{s.t.} & \|\boldsymbol{y}_2\|^2 = 1 \\ & \|\boldsymbol{y}_2-\boldsymbol{c}_0\|^2 \leq \delta \end{cases}, \tag{27}$$

Following the guidelines in [7], [50] and skipping the dependence on $(\boldsymbol{y}_1^{(n-1)}, \boldsymbol{\Delta f}^{(n-1)})$ for simplicity, i.e., $\boldsymbol{\Theta} = \boldsymbol{\Theta}(\boldsymbol{y}_1^{(n-1)}, \boldsymbol{\Delta f}^{(n-1)})$ and $\boldsymbol{M} = \boldsymbol{M}(\boldsymbol{y}_1^{(n-1)}, \boldsymbol{\Delta f}^{(n-1)})$, the homogenized version of $\mathcal{P}_{\boldsymbol{c}^{(n)}}$ is [7]

$$\mathcal{P}'_{\boldsymbol{y}_2^{(n)}}\colon \begin{cases} \max\limits_{\boldsymbol{y}_2, t} & \dfrac{\mathrm{tr}\left(\begin{bmatrix} \boldsymbol{\Theta} & \boldsymbol{0} \\ \boldsymbol{0} & 0 \end{bmatrix}\begin{bmatrix} \boldsymbol{y}_2\boldsymbol{y}_2^\dagger & \boldsymbol{y}_2 t^* \\ \boldsymbol{y}_2^\dagger t & |t|^2 \end{bmatrix}\right)}{\mathrm{tr}\left(\begin{bmatrix} \boldsymbol{M} & \boldsymbol{0} \\ \boldsymbol{0} & 0 \end{bmatrix}\begin{bmatrix} \boldsymbol{y}_2\boldsymbol{y}_2^\dagger & \boldsymbol{y}_2 t^* \\ \boldsymbol{y}_2^\dagger t & |t|^2 \end{bmatrix}\right)} \\ \text{s.t.} & \mathrm{tr}\left(\begin{bmatrix} \boldsymbol{I} & -\boldsymbol{c}_0 \\ -\boldsymbol{c}_0^\dagger & \|\boldsymbol{c}_0\|^2-\delta \end{bmatrix}\begin{bmatrix} \boldsymbol{y}_2\boldsymbol{y}_2^\dagger & \boldsymbol{y}_2 t^* \\ \boldsymbol{y}_2^\dagger t & |t|^2 \end{bmatrix}\right) \leq 0 \\ & \mathrm{tr}\left(\begin{bmatrix} \boldsymbol{I} & \boldsymbol{0} \\ \boldsymbol{0} & 0 \end{bmatrix}\begin{bmatrix} \boldsymbol{y}_2\boldsymbol{y}_2^\dagger & \boldsymbol{y}_2 t^* \\ \boldsymbol{y}_2^\dagger t & |t|^2 \end{bmatrix}\right) = 1 \\ & \mathrm{tr}\left(\begin{bmatrix} \boldsymbol{0} & \boldsymbol{0} \\ \boldsymbol{0} & 1 \end{bmatrix}\begin{bmatrix} \boldsymbol{y}_2\boldsymbol{y}_2^\dagger & \boldsymbol{y}_2 t^* \\ \boldsymbol{y}_2^\dagger t & |t|^2 \end{bmatrix}\right) = 1 \\ & \boldsymbol{y}_2 \in \mathbb{C}^P, t \in \mathbb{C}. \end{cases} \tag{28}$$

Hence, an optimal solution $\boldsymbol{y}_2^{(n)}$ is obtained via two distinct steps, where the former involves the computation of the solution to a SDP problem, while the latter entails the construction of a rank-one optimal solution.

Specifically, at the first step, the problem $\mathcal{P}'_{\boldsymbol{y}_2^{(n)}}$ is relaxed into a fractional SDP problem by dropping the implicit rank-one constraint in (28), i.e.,

$$\tilde{\mathcal{P}}_{\boldsymbol{y}_2^{(n)}}\colon \begin{cases} \max\limits_{\boldsymbol{L}} & \frac{\mathrm{tr}(\boldsymbol{Q}_0\boldsymbol{L})}{\mathrm{tr}(\boldsymbol{Q}_1\boldsymbol{L})} \\ \text{s.t.} & \mathrm{tr}(\boldsymbol{Q}_2\boldsymbol{L}) \leq 0 \\ & \mathrm{tr}(\boldsymbol{Q}_3\boldsymbol{L}) = 1 \\ & \mathrm{tr}(\boldsymbol{Q}_4\boldsymbol{L}) = 1 \\ & \boldsymbol{L} \succeq \boldsymbol{0} \end{cases}, \tag{29}$$

where $\boldsymbol{L} \in \mathbb{H}^{P+1}$. The definitions of $\boldsymbol{Q}_i \in \mathbb{C}^{P+1}$ $(i = 0, \ldots, 4)$ are given in (30).

By resorting to Charnes and Cooper's transformation, and considering that the denominator of the fractional SDP is always positive, an equivalent SDP of $\tilde{\mathcal{P}}_{\boldsymbol{y}_2^{(n)}}$ is obtained as follows

$$\hat{\mathcal{P}}_{\boldsymbol{y}_2^{(n)}}\colon \begin{cases} \max\limits_{\boldsymbol{X}, u} & \mathrm{tr}(\boldsymbol{Q}_0\boldsymbol{X}) \\ \text{s.t.} & \mathrm{tr}(\boldsymbol{Q}_1\boldsymbol{X}) = 1 \\ & \mathrm{tr}(\boldsymbol{Q}_2\boldsymbol{X}) \leq 0 \\ & \mathrm{tr}(\boldsymbol{Q}_3\boldsymbol{X}) = u \\ & \mathrm{tr}(\boldsymbol{Q}_4\boldsymbol{X}) = u \\ & \boldsymbol{X} \succeq \boldsymbol{0}, u \geq 0 \end{cases}, \tag{31}$$

where $\boldsymbol{X} \in \mathbb{H}^{P+1}$ and $u \in \mathbb{R}$ denotes the transformed variable $\boldsymbol{X} = u\boldsymbol{L}$ complying with $\mathrm{tr}(\boldsymbol{Q}_1(u\boldsymbol{L})) = 1$.

Then, starting from an optimal solution $\boldsymbol{X}^\star$ and $u^\star$ to $\hat{\mathcal{P}}_{\boldsymbol{y}_2^{(n)}}$ (whose optimal value is denoted by $v^\star = v(\hat{\mathcal{P}}_{\boldsymbol{y}_2^{(n)}})$), let $\boldsymbol{X}^\star = \frac{\boldsymbol{X}^\star}{u^\star}$, the second step aims at obtaining a rank-one optimal solution $\boldsymbol{x}^\star(\boldsymbol{x}^\star)^\dagger$ resorting to the rank-one matrix decomposition theorems of [43]. Finally, denoting by $\boldsymbol{x}^\star = \left[\boldsymbol{v}^{\star\mathrm{T}}, t^\star\right]^\mathrm{T} \in \mathbb{C}^{P+1}$, with $\boldsymbol{v}^\star \in \mathbb{C}^P$ and $t^\star \in \mathbb{R}^1$, an optimal solution $\boldsymbol{y}_2^{(n)}$ to $\mathcal{P}_{\boldsymbol{y}_2^{(n)}}$ is obtained as [7]

$$\boldsymbol{y}_2^{(n)\star} = \frac{\boldsymbol{v}^\star}{t^\star}. \tag{32}$$

As to $\boldsymbol{x}^\star$, it can be obtained either directly if $\mathrm{Rank}(\boldsymbol{X}^\star) = 1$ (i.e., $\boldsymbol{X}^\star = \boldsymbol{x}^\star\boldsymbol{x}^{\star\dagger}$) or according to [43] if $\mathrm{Rank}(\boldsymbol{X}^\star) > 1$, that is, using Lemma 3 (reported in Appendix E of the supplementary material to this paper and proved in [43]), with $\boldsymbol{A}_1 = \boldsymbol{Q}_0 - v^\star\boldsymbol{Q}_1$, $\boldsymbol{A}_2 = \boldsymbol{Q}_2$, $\boldsymbol{A}_3 = \boldsymbol{Q}_3$, and $\boldsymbol{A}_4 = \boldsymbol{Q}_4$.

C. Receive Filter Optimization

In this case, $h = 1$, and the optimization variable is $\boldsymbol{y}_1$, which is tantamount to solving the following optimization problem

$$\mathcal{P}_{\boldsymbol{y}_1^{(n)}}\colon \begin{cases} \max\limits_{\boldsymbol{y}_1} & \mathrm{SINR}(\boldsymbol{y}_1, \boldsymbol{y}_2^{(n-1)}, \boldsymbol{\Delta f}^{(n-1)}) \\ \text{s.t.} & \|\boldsymbol{y}_1\|^2 = 1 \end{cases}. \tag{33}$$

The optimal solution to $\mathcal{P}_{\boldsymbol{y}_1^{(n)}}$ is obtained according to [7], [51] and is given in (34).

D. Joint Transmit and Receive Optimization Procedure

The joint transmit and receive optimization process is summarized in **Algorithm 2**. To begin with, an admissible code $\boldsymbol{c}^{(0)}$ and frequency increment vector $\boldsymbol{\Delta f}^{(0)}$ are initialized to trigger the optimization procedure for the optimal receiver filter $\boldsymbol{w}^{(0)}$. Specifically, natural choices for the initial frequency increment vector and radar code are respectively linear frequency increment vector, i.e., $\boldsymbol{\Delta f}^{(0)} = [0, \overline{\Delta f}, \ldots, (M-1)\overline{\Delta f}]^\mathrm{T} \in \mathbb{R}^M$ and $\boldsymbol{c}^{(0)} = \boldsymbol{c}_0$, with $\overline{\Delta f} \leq B_w/(M-1)$. In this regard, the process to update each frequency increment, radar code, and receive filter, could be iteratively repeated for a desired number of iterations $N_1 > 0$ or when reaching a convergence condition, e.g.,

$$\left|\chi\left(\boldsymbol{y}^{(n)}\right) - \chi\left(\boldsymbol{y}^{(n-1)}\right)\right| < \varepsilon_1,$$

with $\varepsilon_1 > 0$ the exit threshold, and $\chi(\boldsymbol{y}^{(n)})$ the objective function (12) evaluated at $\boldsymbol{y}^{(n)} = \left[\boldsymbol{y}_1^{(n)\mathrm{T}}, \boldsymbol{y}_2^{(n)\mathrm{T}}, y_3^{(n)}, \ldots, y_{M+2}^{(n)}\right]^\mathrm{T}$.

A schematic representation of the proposed joint transmit-receive optimization procedure is reported in Fig. 2. In this regard, the clutter statistics are retrieved leveraging (possibly dynamically updated) site specific environmental databases, that could include Geographical Information System (GIS), digital terrain maps, meteorological information, and clutter models [7]. Thus, such information is employed to feed the optimization stage thereby designing bespoke filter (receiver side), radar code and frequency increments (transmitter side), with a possible on-line implementation of the proposed algorithm.

This article has been accepted for publication in IEEE Transactions on Signal Processing. This is the author's version which has not been fully edited and content may change prior to final publication. Citation information: DOI 10.1109/TSP.2024.3366438

$$\boldsymbol{Q}_0 = \begin{bmatrix} \boldsymbol{\Theta} & \boldsymbol{0} \\ \boldsymbol{0} & 0 \end{bmatrix}, \boldsymbol{Q}_1 = \begin{bmatrix} \boldsymbol{M} & \boldsymbol{0} \\ \boldsymbol{0} & 0 \end{bmatrix}, \boldsymbol{Q}_2 = \begin{bmatrix} \boldsymbol{I} & -\boldsymbol{c}_0 \\ -\boldsymbol{c}_0^\dagger & \|\boldsymbol{c}_0\|^2 - \delta \end{bmatrix}, \boldsymbol{Q}_3 = \begin{bmatrix} \boldsymbol{I} & \boldsymbol{0} \\ \boldsymbol{0} & 0 \end{bmatrix}, \boldsymbol{Q}_4 = \begin{bmatrix} \boldsymbol{0} & \boldsymbol{0} \\ \boldsymbol{0} & 1 \end{bmatrix}. \tag{30}$$

$$\boldsymbol{y}_1^{(n)\star} = \frac{(\boldsymbol{\Sigma}_c(\boldsymbol{y}_2^{(n-1)}, \boldsymbol{\Delta f}^{(n-1)}) + \sigma_n^2 \boldsymbol{I})^{-1}(\boldsymbol{y}_2^{(n-1)} \otimes \boldsymbol{s}(\theta_0, \Delta\tau, \boldsymbol{\Delta f}^{(n-1)}))}{\sqrt{(\boldsymbol{y}_2^{(n-1)} \otimes \boldsymbol{s}(\theta_0, \Delta\tau, \boldsymbol{\Delta f}^{(n-1)}))^\dagger (\boldsymbol{\Sigma}_c(\boldsymbol{y}_2^{(n-1)}, \boldsymbol{\Delta f}^{(n-1)}) + \sigma_n^2 \boldsymbol{I})^{-2}(\boldsymbol{y}_2^{(n-1)} \otimes \boldsymbol{s}(\theta_0, \Delta\tau, \boldsymbol{\Delta f}^{(n-1)}))}}, \tag{34}$$

Algorithm 1 Joint Transmit and Receive Optimization with MM-MBI.

Input: M, $\overline{\Delta f}$, $\sigma_{l,i,k}^2$, $\boldsymbol{c}_0$, δ, B_w, σ_n^2, N_1.
Output: $\boldsymbol{y}^\star$.

1. Initialization:
   - Set $n = 0$;
   - Set $\boldsymbol{\Delta f}^{(0)} = [0, \overline{\Delta f}, \ldots, (M-1)\overline{\Delta f}]^{\mathrm{T}}$;
   - Set $\boldsymbol{y}_2^{(0)} = \boldsymbol{c}_0$;
   - Compute $\boldsymbol{y}_1^{(0)}$ by (34);
   - Obtain $\boldsymbol{y}^{(0)} = \left[\boldsymbol{y}_1^{(0)\mathrm{T}}, \boldsymbol{y}_2^{(0)\mathrm{T}}, 0, \overline{\Delta f}, \ldots, (M-1)\overline{\Delta f}\right]^{\mathrm{T}}$;
2. **for** $n = 1 : N_1$
3. **for** $h = 3 : M+2$
4. Update $y_h^{(n)}$ according to (23) and denote by $\nu_h^{(n)}$ the corresponding optimal SINR value;
5. **end**
6. Solve for filter $\boldsymbol{y}_1^{(n)}$ and code $\boldsymbol{y}_2^{(n)}$ respectively via (34) and (32), and let $\nu_1^{(n)}$ and $\nu_2^{(n)}$ the optimal values respectively to Problems $\mathcal{P}_{\boldsymbol{y}_1^{(n)}}$ and $\mathcal{P}_{\boldsymbol{y}_2^{(n)}}$;
7. Compute $k^\star = \arg \max_{k=1,\ldots,M+2} \nu_k^{(n)}$;
8. **if** $k^\star \geq 3$
9. Let $\boldsymbol{y}^{(n)} = \left[\boldsymbol{y}_1^{(n-1)\mathrm{T}}, \boldsymbol{y}_2^{(n-1)\mathrm{T}}, \ldots, y_{k^\star}^{(n)}, y_{k^\star+1}^{(n-1)}, \ldots, y_{M+2}^{(n-1)}, \right]^{\mathrm{T}}$;
10. **else**
11. **if** $\nu_h^{(1)} > \nu_h^{(2)}$
12. Let $\boldsymbol{y}^{(n)} = \left[\boldsymbol{y}_1^{(n)\mathrm{T}}, \boldsymbol{y}_2^{(n-1)\mathrm{T}}, y_3^{(n-1)} \ldots, y_{M+2}^{(n-1)}\right]^{\mathrm{T}}$;
13. **else**
14. Let $\boldsymbol{y}^{(n)} = \left[\boldsymbol{y}_1^{(n-1)\mathrm{T}}, \boldsymbol{y}_2^{(n)\mathrm{T}}, y_3^{(n-1)} \ldots, y_{M+2}^{(n-1)}\right]^{\mathrm{T}}$;
15. **end**
16. **end**
17. **end**
18. Output $\boldsymbol{y}^\star = \boldsymbol{y}^{(n)}$.

Notably, a continuous sensing approach to extract clutter statistics could also be conceived. This lends to a potential cognitive implementation, whereby the system alternates perception (environment estimation) and action (transmission of a waveform tailored to the probed environment) in a feedback loop. Precisely, the system updates the clutter statistics by means of a specific sensing stage, possibly performed on a regular basis or on-demand. Then, the inferred clutter characteristics are used to maximize the SINR (12) by optimizing the radar code, the filter, and the frequency increments.

As to the convergence analysis, some relevant properties of the optimization problem $\mathcal{P}$ and **Algorithm 2** are summarized in Proposition 3.

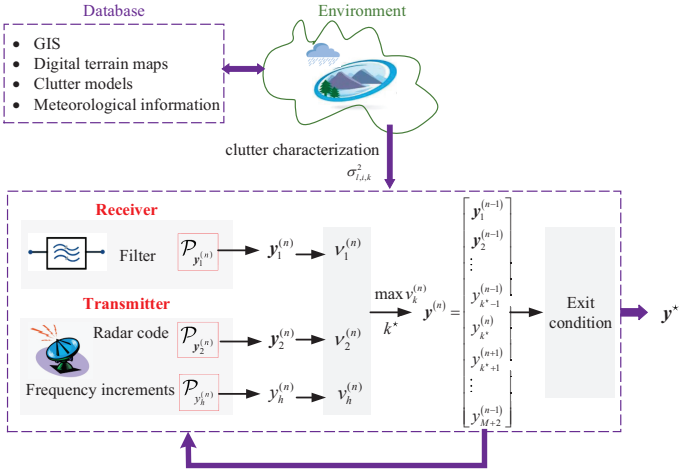

Fig. 2: Block diagram of the transmit-receive optimization procedure.

Proposition 3: The optimization problem $\mathcal{P}$ enjoys the following properties:

- The objective $\chi(\boldsymbol{y})$ is continuous and $\mathcal{P}$ has a compact feasible set. Thus, according to the Weierstrass theorem, $\mathcal{P}$ is solvable[3], and $\chi(\boldsymbol{y}^{(n)}) \leq \upsilon(\mathcal{P})$;
- The objective $\chi(\boldsymbol{y}^{(n)})$ is monotonically increasing and converges to a finite value $\chi^\star$. Moreover, for any cluster point $\boldsymbol{y}^\star$ of $\boldsymbol{y}^{(n)}$, $\chi(\boldsymbol{y}^\star) = \chi^\star$;
- Any cluster point $\boldsymbol{y}^\star$ satisfies the KKT conditions for Problem $\mathcal{P}$.

Proof: See Appendix F of the supplemental material. ■

Notably, another optimization technique that can be used to address the constrained optimization problem (13) is the AO, whereby each block variable is cyclically updated until achieving the desired exit condition [42]. Precisely, problem $\mathcal{P}$ is solved via a MM-Block CD (BCD) technique, which partitions the vector variable into multiple blocks, and then the objective function is alternately improved (either optimized or handled with MM) w.r.t. each block, while keeping the others fixed. In this regard, this alternative optimization process enjoys the same properties as the first and second items of Proposition 3. However, the KKT condition cannot be ensured (in general) for any limit point $\boldsymbol{y}^\star$. Remarkably, the MBI method could also be combined with the sequential optimization theory,

[3]The problem is solvable means it is feasible, bounded above, and its optimal value $\upsilon(\mathcal{P})$ is attained [52].

This article has been accepted for publication in IEEE Transactions on Signal Processing. This is the author's version which has not been fully edited and content may change prior to final publication. Citation information: DOI 10.1109/TSP.2024.3366438

aimed at achieving a better balance between performance and complexity [42].

The computational complexity enrolled in **Algorithm 2** in each iteration lies in the evaluation of the optimized frequency increments (step 4), radar code (step 6), and receive filter (step 6), whose complexities are discussed as follows.

- As to the complexity connected with the frequency increments optimization, the optimal solution to the Problem $\mathcal{P}_{y_h^{(n)}}$ can be accomplished with a complexity of $\mathcal{O}(KIPM^2)$, which corresponds to the computation of the K matrices $\boldsymbol{\Sigma}_k\left(\boldsymbol{w}^{(n-1)}, \boldsymbol{c}^{(n-1)}\right)$.
- As to code design, the complexity lies in solving the SDP $\hat{\mathcal{P}}_{\boldsymbol{y}_2^{(n)}}$, i.e., $\mathcal{O}(P^{3.5}\log(1/\eta))$ with η a predefined accuracy [7], [52]. Moreover, the complexity of the specific rank-one decomposition procedure is $\mathcal{O}(P^3)$. Notably, the optimal value to the corresponding problem requires $\mathcal{O}(1)$ being it obtained as a by product of the SDP procedure;
- As to receive filter optimization, the main complexity is dominated by the computation of $\boldsymbol{\Sigma}_c(\boldsymbol{y}_2^{(n-1)}, \boldsymbol{\Delta f}^{(n-1)})$, which is $\mathcal{O}(P^3M^2N^2IK)$, and the evaluation of the inverse of $\boldsymbol{\Sigma}_c(\boldsymbol{y}_2^{(n-1)}, \boldsymbol{\Delta f}^{(n-1)}) + \sigma_n^2\boldsymbol{I}$, which is $\mathcal{O}((PMN)^3)$. However, since it is positive definite, after the computation of $\boldsymbol{\Sigma}_c(\boldsymbol{y}_2^{(n-1)}, \boldsymbol{\Delta f}^{(n-1)})$, the filter could be efficiently computed resorting to the Conjugate Gradient Method (CGM) [53], with a resulting computational saving. Therefore the overall computational complexity is $\mathcal{O}(P^3M^2N^2(KI + MN))$.

Consequently, the overall computational complexity of each iteration in **Algorithm 2** is $\mathcal{O}\left(P^{3.5}\log(1/\eta) + P^2M^2N^2(KIP + Q)\right)$.

A direct comparison could be useful w.r.t. the AO [7] in terms of computational burden. Specifically in each iteration AO involves solving only one sub-problem yielding a computational complexity of $\mathcal{O}\left(\max\left\{P^{3.5}\log(1/\eta), P^2M^2N^2(KIP + Q)\right\}\right)$. Finally, if a parallel implementation is foreseen for the MBI, the same per-iteration worst case computational burden as per the AO approach is demanded.

Moreover, it is worth noting that the computational burden of some MBI iterations can be mitigated by avoiding redundant evaluations of some terms. For example, the value of $\boldsymbol{\Sigma}_c(\boldsymbol{c}^{(n-1)}, \boldsymbol{\Delta f}^{(n-1)})$ can be reused (by keeping it in memory) until the code or one of the frequency increments is reoptimized. Similarly, the computation of $\boldsymbol{\Sigma}_k\left(\boldsymbol{w}^{(n-1)}, \boldsymbol{c}^{(n-1)}\right)$, $k = 1, \ldots, K$ is demanded only after the optimization of the filter or the code. Indeed, for the same number of iterations, empirical simulations have shown that specific optimization patterns (in terms of MBI selections) can sometimes lead to a computational saving in the MM-MBI implementation as compared to the MM-AO counterpart, due to the larger number of redundant calculations avoided in the former procedure.

Finally, it is worth considering the possibility of parallelizing, at each iteration of the MM-MBI procedure, the optimization of the filter, the code, and the frequency increments, to further reduce the overall computational time.

TABLE I: Simulation Parameters of FDA-MIMO Radar.

Parameter	Value	Parameter	Value
M	4	N	8
B_w	2 MHz	B_c	1 MHz
I	181	L	11
K	5	P	11
σ_n^2	0 dB	N_1	1000

IV. Performance Analysis

In this section, numerical examples are provided to assess the performance of the proposed transceiver design scheme for SINR improvement in an FDA-MIMO radar. The system comprised ULAs for both transmission and reception with $M = 4$ and $N = 8$ elements, respectively, arranged using an inter-element distance equal to half-wavelength. The radar is supposed operating at f_0 = 1 GHz.

In addition, the code length is considered as $P = 11$, and a standard Barker code is used as reference, i.e.,

$$\boldsymbol{c}_0 = [1, 1, 1, -1, -1, -1, 1, -1, -1, 1, -1]^{\mathrm{T}} \tag{35}$$

and $\delta = 0.5$ is employed unless otherwise specified.

Moreover, a linear pattern is considered to initialize the carrier frequencies of the M transmit elements [31], using a constant frequency increment of $\overline{\Delta f}$ = 0.5 MHz, namely,

$$\boldsymbol{\Delta f}^{(0)} = [0, 0.5, 1, 1.5]^{\mathrm{T}}\text{MHz}, \tag{36}$$

whereas the available radar bandwidth is assumed to be B_w = 2 MHz.

As to the clutter, two different heterogeneous environments, with mixed ground/sea clutter, are examined, thereby assuming their statistical characterization known *a priori*, e.g., retrieved through a geographic-query to a site specific environmental database [7]. The former refers to the case of typical clutter edges scenario while in the latter different clutter patches are considered located at specific azimuth sectors. In both cases, it is employed a discretization of the azimuthal domain in I = 181 sectors (see Fig. 1), while considering $L = 11$ range rings interfering with the range-azimuth bin of interest (BOI), i.e., $(0, 0)$. The setup parameters involved in the simulations are listed in Table I, whereby the target incremental range is assumed to be $\Delta\tau = 1/(10B_c)$.

At each iteration, the normalized SINR achieved with the proposed MM-MBI and MM-AO algorithms are compared with three counterparts: two simpler MBI approaches, i.e.,

- MBI optimizing only the transmitted code and the receive filter (referred to as MBI-C&F), whose corresponding design problem is

$$\mathcal{P}_{\boldsymbol{w},\boldsymbol{c}}: \begin{cases} \max\limits_{\boldsymbol{w},\boldsymbol{c}} & \mathrm{SINR}(\boldsymbol{w}, \boldsymbol{c}, \boldsymbol{\Delta f}^{(0)}) \\ \text{s.t.} & \|\boldsymbol{w}\|^2 = 1 \\ & \|\boldsymbol{c}\|^2 = 1 \\ & \|\boldsymbol{c} - \boldsymbol{c}_0\|^2 \le \delta \end{cases}; \tag{37}$$

- MBI optimizing only the frequency increments and the receive filter (referred to as MBI-DF&F), whose corre-

This article has been accepted for publication in IEEE Transactions on Signal Processing. This is the author's version which has not been fully edited and content may change prior to final publication. Citation information: DOI 10.1109/TSP.2024.3366438

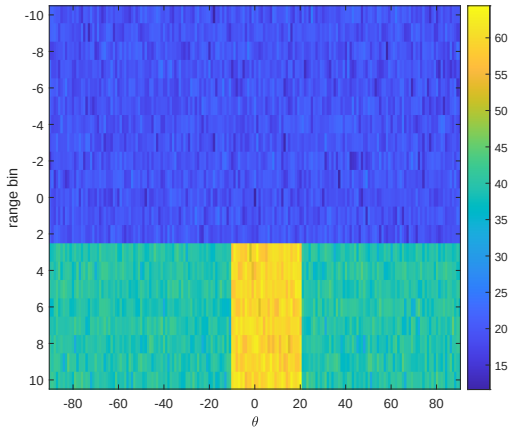

Fig. 3: Clutter power distribution (dB) of subsection IV-A, i.e., an heterogeneous environment with clutter edges.

sponding resource allocation problem is

$$\mathcal{P}_{\boldsymbol{w},\boldsymbol{\Delta f}}: \begin{cases} \max\limits_{\boldsymbol{w},\boldsymbol{\Delta f}} & \mathrm{SINR}(\boldsymbol{w}, \boldsymbol{c}_0, \boldsymbol{\Delta f}) \\ \text{s.t.} & \|\boldsymbol{w}\|^2 = 1 \\ & 0 \le \Delta f_m \le B_w,\ m = 1, \cdots, M \end{cases}, \tag{38}$$

- and a receive-only adaptation for a fixed code and frequency increments (referred to as OPT-FLT), i.e.,

$$\boldsymbol{w}_{\mathrm{OPT-FLT}} = \begin{array}{l} \arg\max\limits_{\boldsymbol{w}} \mathrm{SINR}(\boldsymbol{w}, \boldsymbol{c}_0, \boldsymbol{\Delta f}^{(0)}) \\ \text{s.t. } \|\boldsymbol{w}\|^2 = 1 \end{array} \tag{39}$$

which is computed via the RHS of (34) with $n = 1$.

A. Heterogeneous Environment with Clutter Edges

In the following, an heterogeneous clutter environment encompassing clutter edges is considered. The specific case study at hand is represented in Fig. 3, which reports, for each range-azimuth bin, the sum of the mean square values of the K clutter scatterers, i.e., $\sum_{k=1}^{K} |n_{l,i,k}|^2$. More precisely,

$$\sigma_{l,i,k}^2 = \mathrm{CNR}_{l,i} |n_{l,i,k}|^2, \tag{40}$$

with $\mathrm{CNR}_{l,i}$ = 10dB in the range rings from -11 to 2, while for the other rings the clutter profile is considered having $\mathrm{CNR}_{l,i}$ = 50 dB within the region $[-10°, 20°]$ and $\mathrm{CNR}_{l,i}$ = 30 dB elsewhere, whereas $n_{l,i,k}$ is a zero-mean, unit-variance, complex Gaussian random variable.

The obtained results, depicted in Fig. 4, demonstrate substantial SINR improvements achievable through the joint optimization of the transmit DOFs, i.e., the radar code and frequency increments, and the receive filter. A careful study of the curves in Fig. 4 (a) reveals that the proposed MM-MBI and MM-AO algorithms can significantly enhance the SINR, with MM-MBI outperforming all the counterparts. Specifically, at the 200-th iteration, MM-MBI achieves a remarkable SINR gain of 5.75 dB, with a gap of 0.22 dB w.r.t. MM-AO. Moreover, MM-MBI shows faster convergence (achieved at ≈ 700 iterations), compared to MM-AO (reaching convergence at ≈ 900 iterations).

Furthermore, it is observed that the MM-MBI exhibits, at the 1000-th iteration, some SINR improvement as compared

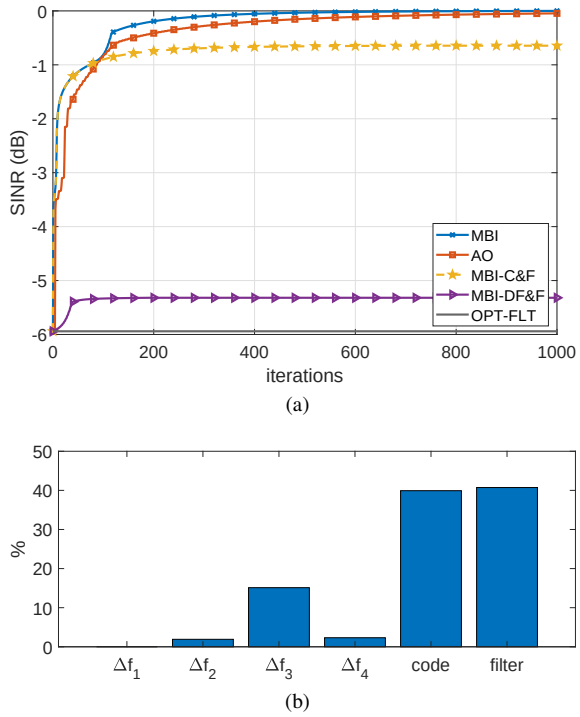

Fig. 4: Optimization results for the first environmental scenario: (a) Normalized SINR versus the number of iterations; (b) Percentage of MBI selections.

with the MBI-C&F and MBI-DF&F approaches, with gaps in the order of 0.64 dB and 5.32 dB, respectively. Additionally, Fig. 4 (b) shows the percent of times each block variable is optimized by the devised MM-MBI procedure. Evidently, the chart underscores, for this case study, a prevailing emphasis on code and filter optimizations rather than on frequency increments.

To shed light on the role of code optimization, in Fig. 5, the normalized SINR versus the number of iterations of the MBI-based optimization is reported for several values of the similarity constraint, i.e., $\delta \in \{0.1, 0.3, 0.5, 0.7\}$. Not surprisingly, a higher value of δ leads to a better SINR gain due to a less stringent constraint on the code optimization, with gap (at the 1000-th iteration) of approximately 3 dB between the cases of $\delta = 0.7$ and $\delta = 0.1$. However, this advantage comes with the potential drawback of losing control over certain critical characteristics of the reference waveform. Furthermore, the results show that larger values of δ demand an increased number of iterations to achieve convergence.

Fig. 6 reports the range-angle system response, i.e.,

$$|\boldsymbol{w}^{(n)\dagger} \boldsymbol{v}_{l,i}|^2,\ l = -L+1, \ldots, L-1,\ i = 0, \ldots, I-1, \tag{41}$$

with $\boldsymbol{v}_{l,i} = \boldsymbol{J}_l \boldsymbol{c}^{(n)} \otimes \boldsymbol{s}(\theta_i, \Delta\tau_k, \boldsymbol{\Delta f}^{(n)})$, corresponding to the strength of filter output to the echo of a possible target located at θ_i and the l-th range ring, with the radar system using the optimized transceiver at a specific iteration of the MM-MBI algorithm. The results, achieved with the initialized parameters, 4-th, 100-th, and 1000 iterations, are illustrated in Figs. 6 (a)-(d), respectively. Inspection of the figures reveals that the proposed optimization strategy is effectively able to preserve the response at the target's bin, i.e., $0°$ and $L = 0$,

This article has been accepted for publication in IEEE Transactions on Signal Processing. This is the author's version which has not been fully edited and content may change prior to final publication. Citation information: DOI 10.1109/TSP.2024.3366438

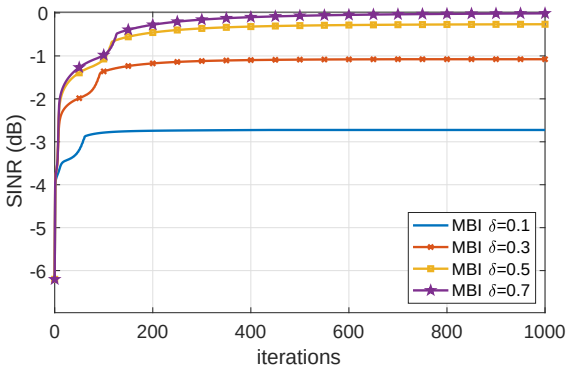

Fig. 5: Normalized SINR (assuming different values of δ) versus iteration using the MBI-based optimization, with $\delta \in \{0.1, 0.3, 0.5, 0.7\}$.

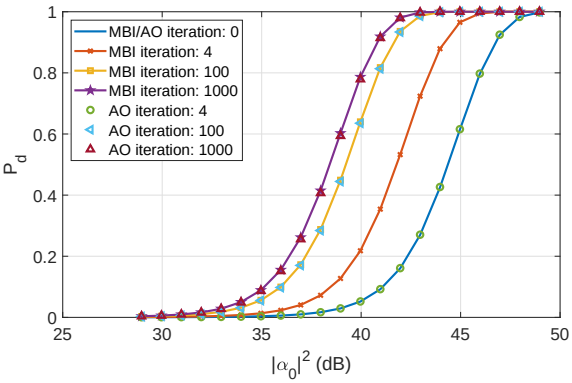

Fig. 7: Detection probability at a given iteration for the first environmental scenario.

while minimizing that at other locations, in particular after 100 iterations. Such behavior corroborates the capability of the developed joint transmit-receive optimization procedure to suppress the clutter and improve the SINR.

Now, assuming the case of non-fluctuating (Swerling 0) target, the probability of detection ($\mathrm{P_d}$) for the coherent detector

$$|\boldsymbol{w}^{\dagger}\boldsymbol{v}| \underset{\mathcal{H}_0}{\overset{\mathcal{H}_1}{\gtrless}} \zeta \tag{42}$$

is given by

$$Q\left(\sqrt{2|\alpha_0|^2\hat{\chi}}, \sqrt{-2\log \mathrm{P_{fa}}}\right), \tag{43}$$

where $\mathcal{H}_0$ and $\mathcal{H}_1$ indicate the null and the alternative hypothesis (i.e., target echo absence/presence within the received observation vector), respectively, ζ is the detection threshold set to ensure the desired false alarm probability ($\mathrm{P_{fa}}$), $Q(\cdot)$ is the Marcum Q function [54], and $\hat{\chi}$ is the achieved normalized SINR after the joint transmit-receive optimization.

The $\mathrm{P_d}$ versus $|\alpha_0|^2$, for $\mathrm{P_{fa}} = 10^{-4}$, at different iterations of the devised MM-MBI procedure, is displayed in Fig. 7 assuming the same interference environment as in Fig. 3. The curves highlight that, for a given $|\alpha_0|^2$, increasing the number of iterations leads to a better $\mathrm{P_d}$, owing to the achieved higher normalized SINR. Moreover, the MBI approach yields superior performance than the AO counterpart, in particular with designs after a small number of iterations.

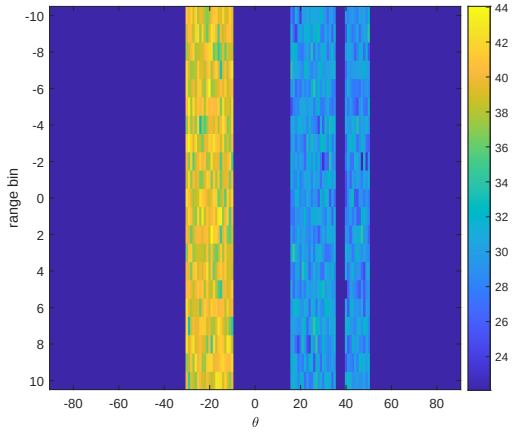

Fig. 8: Clutter power distribution (dB) of subsection IV-B, i.e., an heterogeneous environment with clutter patches.

B. Heterogeneous Environment with Clutter Patches

The second analyzed environmental scenario still assumes clutter powers modeled as in (40) but it encompasses three different patches arranged in the following patterns: $[-30°, -10°]$ with $\mathrm{CNR}_{l,i}$ = 30 dB, $[15°, 35°]$ with $\mathrm{CNR}_{l,i}$ = 20 dB, and $[40°, 50°]$ with $\mathrm{CNR}_{l,i}$ = 20 dB, respectively. The corresponding clutter profile is illustrated in Fig. 8.

The optimization results are displayed in Fig. 9 in terms of achieved normalized SINR in Fig. 9 (a), and MBI parameter selection count in Fig. 9 (b). Similar to the preceding case, the MBI-based strategy demonstrates superior performance than the other approaches, achieving the highest SINR gain of 4.23 dB. Notably, the results emphasize that, in this specific study case, the primary contributor to the SINR gain is the optimization of the frequency increments. This observation is supported by both the data depicted in Fig. 9 (b) and the performance achieved by the MBI-DF&F, which, in terms of normalized SINR, ranks second. Furthermore, the MBI-C&F approach fails to yield any SINR improvement, mainly due to the absence of frequency increments optimization in its design.

The squared modulus of the filter response (41), computed with the nominal parameters as well as with the optimized ones at 4-th, 100-th and final iterations, is displayed in Figs. 10 (a)-(d), respectively. From the maps at different iterations, it is possible to observe that an effective clutter suppression, in both range and azimuth domains, is achieved with the devised optimization strategy.

The $\mathrm{P_d}$ (43) versus $|\alpha_0|^2$ is plotted in Fig. 11 for the normalized SINR values achieved by the MM-MBI and MM-AO procedures at specific iterations, i.e., before the optimization (0-th), 4-th, 100-th, and 1000-th. As expected, an increase of $\mathrm{P_d}$ is attained with a large number of iterations, that is, due to the SINR gain obtained with the optimization procedures.

Finally, remarks similar to those made for Fig. 8, i.e., the detection probability results under the first environmental scenario, hold true with reference to the curves displayed in Fig. 11. Precisely, regardless of the number of iteration, the results highlight a slight advantage of MM-MBI procedure over the MM-AO counterpart, with gaps between the curves less than 0.5 dB.

This article has been accepted for publication in IEEE Transactions on Signal Processing. This is the author's version which has not been fully edited and content may change prior to final publication. Citation information: DOI 10.1109/TSP.2024.3366438

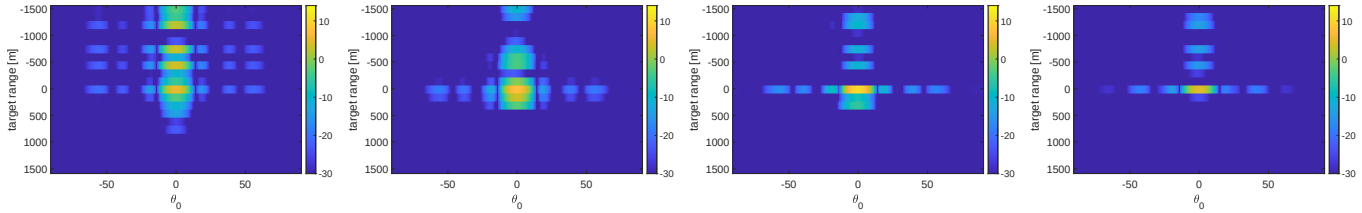

Fig. 6: Squared modulus (dB) of the filter response at a given range azimuth position for the first environmental scenario and iteration: (a) Initial; (b) 4-th iteration; (c) 100-th iteration; (d) 1000-th iteration.

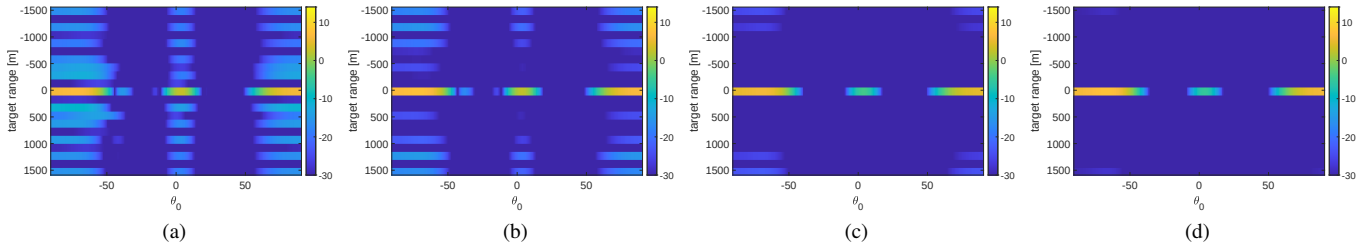

Fig. 10: Squared modulus (dB) of the filter response at a given range azimuth position for the second environmental scenario and iteration: (a) Initial; (b) 4-th iteration; (c) 100-th iteration; (d) 1000-th iteration.

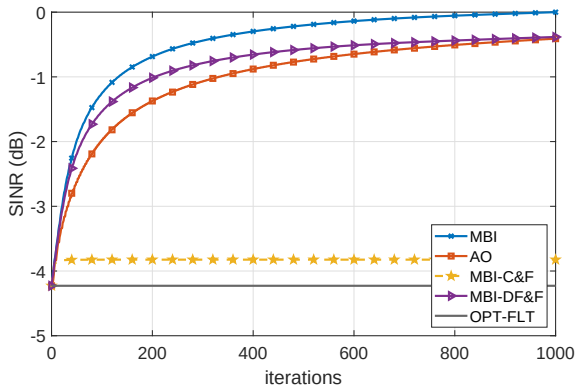

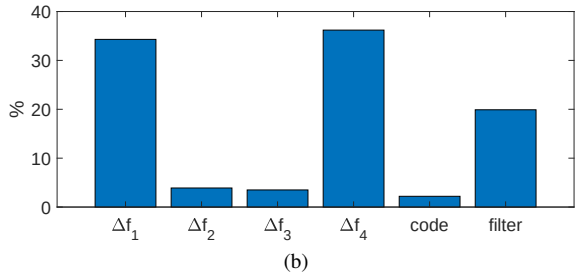

Fig. 9: Optimization results for the second environmental scenario: (a) Normalized SINR versus the number of iterations; (b) Percentage of MBI selections.

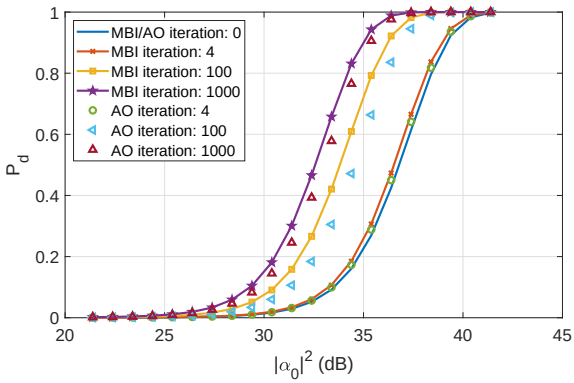

Fig. 11: Detection probability at a given iteration for the second environmental scenario.

V. Conclusions

This paper has dealt with the problem of joint transmitter and receiver synthesis in a signal-dependent interference environment using an FDA-MIMO radar system. The adopted design leverages the SINR maximization over the receiving filter, the radar code, and the FDA frequency increments under some system constraints ruled by the available transmit energy, code features, and total bandwidth. Since the resulting optimization problem is in general non-convex and NP-hard, to come up with good quality solutions, a bespoke optimization framework based on the MM-MBI approach has been proposed and assessed. Specifically, at each iteration, the devised iterative procedure outputs the triple: optimized radar code, frequency increments, and receive filter exploiting the MM methodology. The convergence properties of the algorithm have been rigorously proven showing that any cluster point satisfies the KKT conditions. Moreover, the overall computational complexity has been evaluated and discussed. At the analysis stage, the performance of the joint transceiver optimization technique is analyzed via diverse metrics, including the SINR versus the number of iterations, the detection probability, and the interference cancellation capabilities realized at the output of the receive filter. In this respect, numerical results have demonstrated that the proposed algorithm can effectively suppress the signal-dependent clutter leading to significant SINR improvements as the number of iterations increases. Additionally, comparisons with other design methods, includ-

ing MM-AO and two simpler MBIs optimizing only a subset of the available DOFs, further corroborate the performance enhancements achievable capitalizing the full flexibility of the system.

Possible future research avenues could be focused on the extension of the framework to the case of space-(slow) time processing, where spatial processing is jointly performed together with a Doppler processing, as well as to a polarimetric FDA-MIMO system. Moreover, it could be of interest to consider the structured case of a uniform FDA increment from sensor to sensor and optimize just a single frequency parameter. Last but not least, it is worthy mentioning the possibility to endow robustness to the transceiver performance w.r.t. some unavoidable mismatches induced by coupling effects [55] and pointing errors [56]. Finally, an experimental validation undoubtedly represents the final benchmark to claim the effectiveness of the approach.

REFERENCES

[1] A. De Maio, S. D. Nicola, Y. Huang, S. Zhang, and A. Farina, "Code design to optimize radar detection performance under accuracy and similarity constraints," *IEEE Trans. Signal Process.*, vol. 56, no. 11, pp. 5618-5629, Nov. 2008.

[2] L. Wu, P. Babu, and D. P. Palomar, "Transmit waveform/receive filter design for MIMO radar with multiple waveform constraints," *IEEE Trans. Signal Process.*, vol. 66, no. 6, pp. 1526-1540, Dec. 2018.

[3] P. Stoica, H. He, and J. Li, "Optimization of the receive filter and transmit sequence for active sensing," *IEEE Trans. Signal Process.*, vol. 60, no. 4, pp. 1730-1740, Apr. 2012.

[4] M. Alaee-Kerahroodi, L. Wu, E. Raei, and M. R. B. Shankar, "Joint waveform and receive filter design for pulse compression in weather radar systems," *IEEE Trans. Signal Process.*, vol. 1, pp. 212-229, June 2023.

[5] M. M. Naghsh, M. Soltanalian, P. Stoica, and M. Modarres-Hashemi, "Radar code design for detection of moving targets," *IEEE Trans. Aerosp. Electron. Syst.*, vol. 50, no. 4, pp. 2762-2778, Oct. 2014.

[6] A. Aubry, A. De Maio, M. Piezzo, A. Farina, and M. Wicks, "Cognitive design of the transmitted phase code and receive filter in reverberating environment," *2012 International Waveform Diversity & Design Conference (WDD)*, Kauai, HI, USA, 2012.

[7] A. Aubry, A. De Maio, A. Farina, and M. Wicks, "Knowledge-aided (potentially cognitive) transmit signal and receive filter design in signal-dependent clutter," *IEEE Trans. Aerosp. Electron. Syst.*, vol. 49, no. 1, pp. 93-117, Jan. 2013.

[8] M. Soltanalian, B. Tang, J. Li, and P. Stoica, "Joint design of the receive filter and transmit sequence for active sensing," *IEEE Signal Process. Letters*, vol. 20, no. 5, pp. 423-426, May 2013.

[9] M. M. Naghsh, M. Soltanalian, P. Stoica, M. Modarres-Hashemi, A. De Maio, and A. Aubry, "A Doppler robust design of transmit sequence and receive filter in the presence of signal-dependent interference," *IEEE Trans. Signal Process.*, vol. 62, no. 4, pp. 772-785, Feb. 2014.

[10] B. Tang, J. Tuck, and P. Stoica, "Polyphase waveform design for MIMO radar space time adaptive processing," *IEEE Trans. Signal Process.*, vol. 68, pp. 2143-2154, Mar. 2020.

[11] X. Yu, G. Cui, L. Kong, J. Li, and G. Gui, "Constrained waveform design for colocated MIMO radar with uncertain steering matrices," *IEEE Trans. Aerosp. Electron. Syst.*, vol. 55, no. 1, pp. 356-370, Feb. 2019.

[12] G. Cui, X. Yu, V. Carotenuto, and L. Kong, "Space-time transmit code and receive filter design for colocated MIMO radar," *IEEE Trans. Signal Process.*, vol. 65, no. 5, pp. 1116-1129, Mar. 2017.

[13] A. De Maio, S. De Nicola, Y. Huang, Z.-Q. Luo, and S. Zhang, "Design of phase codes for radar performance optimization with a similarity constraint," *IEEE Trans. Signal Process.*, vol. 57, no. 2, pp. 610-621, Feb. 2009.

[14] A. De Maio, Y. Huang, M. Piezzo, S. Zhang, and A. Farina, "Design of optimized radar codes with a peak to average power ratio constraint," *IEEE Trans. Signal Process.*, vol. 59, no. 6, pp. 2683-2697, June 2011.

[15] Y. Sun, P. Babu, and D. P. Palomar, "Majorization-minimization algorithms in signal processing, communications, and machine learning," *IEEE Trans. Signal Process.*, 65(3): 794-816, Nov. 2016.

[16] X. Du and C. Wei. "Sequential optimization and reliability assessment method for efficient probabilistic design," *J. Mech. Des.* 126(2): 225-233, 2004.

[17] N. Halko, P. G. Martinsson, and J. A. Tropp. "Finding structure with randomness: Probabilistic algorithms for constructing approximate matrix decompositions," *SIAM review*, 53(2), 217-288, 2011.

[18] S. J. Wright, "Coordinate descent algorithms," *Math. Programm.*, vol. 151, no. 1, pp. 3-34, 2015.

[19] B. Tang and J. Tang, "Joint design of transmit waveforms and receive filters for MIMO radar space-time adaptive processing," *IEEE Trans. Signal Process.*, vol. 64, no. 18, pp. 4707-4722, 15 Sept.15, May 2016.

[20] M. M. Feraidooni, D. Gharavian, M. Alaee-Kerahroodi, and S. Imani, "A coordinate descent framework for probing signal design in cognitive MIMO radars," *IEEE Commun. Lett.*, vol. 24, no. 5, pp. 1115-1118, May 2020.

[21] J. Yang, A. Aubry, A. De Maio, X. Yu, and G. Cui, "Multi-spectrally constrained transceiver design against signal-dependent interference, *IEEE Trans. Signal Process.*, vol. 70, pp. 1320-1332, Jan. 2022.

[22] A. Aubry, A. De Maio, M. Piezzo, M. M. Naghsh, M. Soltanalian, and P. Stoica, "Cognitive radar waveform design for spectral coexistence in signal-dependent interference," 2014 IEEE Radar Conference, Cincinnati, OH, USA, 2014, pp. 0474-0478.

[23] P. Stoica, J. Li, and Y. Xie, "On probing signal design for MIMO radar," *IEEE Trans. Signal Process.*, vol. 55, no. 8, pp. 4151-4161, July 2007.

[24] J. Li and P. Stoica, *MIMO radar signal processing*, John Wiley & Sons, 2008.

[25] C.-Y. Chen and P. Vaidyanathan, "MIMO radar waveform optimization with prior information of the extended target and clutter," *IEEE Trans. Signal Process.*, vol. 57, no. 9, pp. 3533-3544, Sep. 2009.

[26] E. Raei, M. Alaee-Kerahroodi, P. Babu, and M. R. B. Shankar, "Generalized waveform design for sidelobe reduction in MIMO radar systems," *Signal Process.*, vol. 206, 108914, May 2013.

[27] S. M. Karbasi, A. Aubry, V. Carotenuto, M. M. Naghsh, and M. H. Bastani, "Knowledge-based design of space-time transmit code and receive filter for a multiple-input-multiple-output radar in signal-dependent interference, *IET Radar Sonar Navig.*, vol. 9, no. 8, pp. 1124-1135, Apr. 2015.

[28] G. Cui, A. De Maio, A. Farina, and J. Li, *Radar waveform design based on optimization theory*, IET Radar Sonar Navig., 2020.

[29] E. Raei, M. Alaee-Kerahroodi, and M. R. B. Shankar, "Spatial- and range- ISLR trade-off in MIMO radar via waveform correlation optimization," *IEEE Trans. Signal Process.*, vol. 69, pp. 3283-3298, May 2021.

[30] M. Wang, X. Li, L. Gao, Z. Sun, G. Cui, and T. S. Yeo, "Signal accumulation method for high-speed maneuvering target detection Using airborne coherent MIMO radar," *IEEE Trans. Signal Process.*, vol. 71, pp. 2336-2351, June 2023.

[31] P. Antonik, M. C. Wicks, H. D. Griffiths, and C. J. Baker, "Frequency diverse array radars," 2006 IEEE Conference on Radar, Verona, NY, USA, 2006, pp. 1-3.

[32] W. Jia, W.-Q. Wang, and S. Zhang, "Joint design of the transmit and receive weights for coherent FDA radar," *Signal Process.*, vol. 204, pp. 1-9, Nov. 2022.

[33] N. Rubinstein and J. Tabrikian, "Frequency diverse array signal optimization: from non-cognitive to cognitive radar," *IEEE Trans. Signal Process.*, vol. 69, pp. 6206-6220, Oct. 2021.

[34] L. Lan, A. Marino, A. Aubry, A. De Maio, G. Liao, J. Xu, and Y. Zhang, "GLRT-based adaptive target detection in FDA-MIMO radar," *IEEE Trans. Aerosp. Electron. Syst.*, vol. 57, no. 1, pp. 597-613, Feb. 2021.

[35] P. F. Sammartino, C. J. Baker, and H. D. Griffiths, "Frequency diverse MIMO techniques for radar," *IEEE Trans. Aerosp. Electron. Syst.*, vol. 49, no. 1, pp. 201-222, Jan. 2013.

[36] L. Lan, J. Xu, G. Liao, Y. Zhang, F. Fioranelli, and H.-C. So, "Suppression of mainbeam deceptive jammer with FDA-MIMO radar," *IEEE Trans Veh. Tech.*, vol. 69, no. 10, pp. 11584-11598, Oct. 2020.

[37] J. Xu, G. Liao, Y. Zhang, H. Ji, and L. Huang, "An adaptive range-angle-Doppler processing approach for FDA-MIMO radar using three-dimensional localization," *IEEE J. Sel. Topics Signal Process.*, vol. 11, no. 2, pp. 309-320, Mar. 2017.

[38] C. Wen, M. Tao, J. Peng, J. Wu, and T. Wang, "Clutter suppression for airborne FDA-MIMO radar using multi-waveform adaptive processing and auxiliary channel STAP," *Signal Process.*, vol. 154, pp. 280-293, Jan. 2019.

[39] C. Wen, C. Ma, J. Peng, and J. Wu, "Bistatic FDA-MIMO radar space-time adaptive processing," *Signal Process.*, vol. 163, pp. 201-212, Jan. 2019.

[40] C. Zhou, C. Wang, J. Gong, M. Tan, L. Bao, and M. Liu, "Joint optimisation of transmit beamspace and receive filter in frequency diversity array-multi-input multi-output radar," *IET Radar Sonar Navig.*, vol. 16, pp. 2031-2039, Aug. 2022.

[41] Z. Ding and J. Xie, "Joint transmit and receive beamforming for cognitive FDA-MIMO radar with moving target," *IEEE Sensors J.*, vol. 21, no. 18, pp. 20878-20885, Sept. 2021.

[42] A. Aubry, A. De Maio, A. Zappone, M. Razaviyayn, and Z.-Q. Luo, "A new sequential optimization procedure and its applications to resource allocation for wireless systems," *IEEE Trans. Signal Process.*, vol. 66, no. 24, pp. 6518-6533, Dec. 2018.

[43] W. Ai, Y. Huang, and S. Zhang, "New results on Hermitian matrix rank-one decomposition," *Math. Program*, Aug. 2009.

[44] D. P. Bertsekas, *Nonlinear Programming*, 2nd ed. Belmont, MA, USA: Athena Scientific, 1999.

[45] L. Lan, M. Rosamilia, A. Aubry, A. De Maio, and G. Liao, "Single-snapshot angle and incremental range estimation for FDA-MIMO radar," *IEEE Trans. Aerosp. Electron. Syst.*, vol. 57, no. 6, pp. 3705-3718, May 2021.

[46] A. Farina, A. De Maio, and S. Haykin, *The impact of cognition on radar technology*, Edison, NJ: SciTech, 2017.

[47] M. Razaviyayn, M. Hong, and Z.-Q. Luo, "A unified convergence analysis of block successive minimization methods for nonsmooth optimization," *SIAM J. Optimization*, vol. 23, no. 2, pp. 1126-1153, 2013.

[48] A. Aubry, A. De Maio, M. A. Govoni, and L. Martino, "On the design of multi-spectrally constrained constant modulus radar signals," *IEEE Trans. Signal Process.*, vol. 68, pp. 2231-2243, Apr. 2020.

[49] A. Aubry, P. Babu, A. De Maio, G. Fatima, and N. Sahu, "A robust framework to design optimal sensor locations for TOA or RSS source localization techniques," *IEEE Trans. Signal Process.*, Mar. 2023.

[50] A. De Maio, Y. Huang, D. P. Palomar, S. Zhang, and A. Farina, "Fractional QCQP with applications in ML steering direction estimation for radar detection," *IEEE Trans. Signal Process.*, vol. 59, no. 1, pp. 172-185, Jan. 2011.

[51] H. L. Van Trees, *Optimum Array Processing: Part IV*, Detection, Estimation, and Modulation Theory. Hoboken, NJ, USA: Wiley, 2004.

[52] A. Ben-Tal and A. Nemirovski, *Lecture on modern convex optimization: Analysis, algorithms, and engineering applications*. Philadelphia, PA, USA: MPS-SIAM, 2001.

[53] J. R. Shewchuk, "An introduction to the conjugate gradient method without the agonizing pain," Carnegie Mellon Univ., 1994.

[54] J. Marcum, "A statistical theory of target detection by pulsed radar," *IRE Trans. on Inf. Theory*, vol. 6, no. 2, pp. 59-267, Apr. 1960.

[55] A. Aubry, A. De Maio, L. Lan, and M. Rosamilia, "Adaptive radar detection and bearing estimation in the presence of unknown mutual coupling," *IEEE Trans. Signal Process.*, vol. 71, pp. 1248-1262, Mar. 2023.

[56] A. Aubry, A. De Maio, S. Marano, and M. Rosamilia, "Single-pulse simultaneous target detection and angle estimation in a multichannel phased array radar," *IEEE Trans. Signal Process.*, vol. 68, pp. 6649-6664, Nov. 2020.